Small Monopropellant Thruster Contamination Measurement in a High-Vacuum Low-Temperature Facility

R.S. Passamaneck* and J.E. Chirivella†
Jet Propulsion Laboratory, Pasadena, Calif.

The contamination that results from the exhaust plume of small thrusters used for attitude control maneuvers can pose severe problems for long-lift satellite systems. In order to assess this type of contamination problem, analytical and experimental techniques must be developed. Mass deposition rate measurements of a representative 0.44-N thrust hydrazine thruster were made in the Jet Propulsion Laboratory (JPL) Molsink space simulation chamber using five appropriately placed variable-temperature quartz crystal microbalances. The mass deposition rates within the thruster plume were measured while operating the thruster over a wide range of operating parameters, including duty cycles, catalyst bed start temperatures, propellant water variation, as well as thruster aging effects. The contamination measurements were made over a temperature range of 144 to 256 K for all duty cycles. In addition, the nominal duty cycle of 100 msec on and 10 sec off was run at a temperature of 106 K. These data will make possible better prediction of deposition rates of contaminants from thrusters used in satellite systems.

Introduction

THERE is the potential of contamination of sensitive surfaces on a spacecraft such as thermal coatings, optics, and solar panels by direct mass deposition when a thruster fires in space. The prediction of the contamination rate and location is very complex and difficult. Therefore, the development of the capability to provide basic experimental data and to verify the advanced, computerized models used in the analysis is a required major step in the studies of those processes leading to the prediction of contamination, as well as its effects on the properties of spacecraft surfaces.

When a monopropellant hydrazine engine is fired in a vacuum, hydrogen, nitrogen, and ammonia are the main exhaust products. The concentration of these gases depends on the percentage of decomposition of the ammonia, which is dictated by performance considerations. Other species also are present in the exhaust. Because of the chemical process used in the preparagion of hydrazine, traces of water and aniline up to a total of 1% are accepted. The aniline probably becomes a hydrocarbon, and water may remain water or become ammonium hydrates in passing through the catalyst bed. Small amounts of unreacted hydrazine also have been found consistently in chemical analysis of the exhaust gases. Although the water, aniline, and unreacted hydrazine constitute a small percentage of the exhaust gases, they are most likely the main contributors to contamination, since they condense on surfaces at much higher temperatures than the plentiful gases hydrogen, nitrogen, and ammonia.

This paper describes a series of tests that have been conducted to assess the contamination potential of a small hydrazine engine. A Hamilton-Standard (REA 10-18) 0.44-N hydrazine thruster was used for these tests and operated by firing it vertically downward in an ultrahigh vacuum chamger (Molsink). The thruster was fired in a pulse mode. Pulse widths of 25, 100, and 200 msec with off-times of 5, 10, and 20 sec, respectively, were investigated.

Catalyst bed temperatures at the start of the tests varied from 295 to 590 K, with the bulk of the testing at 477 K. The propellant, which assayed at 0.7% water, was the same for all tests with the exception of a few tests in which nominally 1% water by weight was added to assess the effect of water on contamination. Quartz crystal microbalances (QCM's) were used to measure mass deposition. Five QCM's were mounted approximately 1.1 m below the engine to measure contamination from the exhaust plume and were operated at temperatures from 106 to 256 K. Mass deposition rates on the order of 10^{-8} g/(cm^2-sec) at 106 K, where some ammonia condensation is expected, to 10^{-11} g/(cm^2-sec) at 256 K, where only some aniline and water contribute to contamination, were seen.

Received July 26, 1976; revision received Feb. 18, 1977.
Index categories: Fuels and Propellants, Properties of; Liquid Rocket Engines and Missile Systems.

*Currently Assistant Professor, Department of Mechanical Engineering, University of New Mexico, Albuquerque, N. Mex.
†Member of the Technical Staff, Energy and Materials Research Section.

Experimental Vacuum Facility

Proper evaluation of the experiment and a deeper insight into the results requires a general understanding of the Molsink facility and its working principles. A major problem associated with the study of rocket exhaust plumes and contamination is the sensitivity of the measurements to recirculation effects in the space simulator. Since the measurements that this work deals with are mass deposition rates of contaminants, the Molsink facility was selected as it is an ultrahigh vacuum chamber capable of cryopumping injected gases at a very high rate, which would keep recirculation to a minimum. This facility consists of a vacuum chamber and associated cryogenic and vacuum systems. The vacuum chamber encloses two other chambers: the inner liner and the molecular trap. The inner liner is filled with liquid nitrogen that acts as a massive heat sink. The molecular trap, the innermost chamber, is a sphere of approximately 3 m diam, maintained at a temperature of about 10 K with gaseous helium. The aluminum moltrap walls are wedge-shaped, resembling an anechoic chamber, with a total surface area of 186 m^2. Liquid nitrogen is supplied to the inner liner from a central tank and vented to the atmosphere. The moltrap is cooled by a manifold of tubes, within which gaseous helium circulates at approximately 7 K. The helium is kept at this very low temperature by a refrigerator located adjacent to the chamber. The chamber walls also are coated with titanium, which acts as a "getter" material to trap helium and hydrogen that are not cryopumped by the 10 K surfaces. The amount of helium and hydrogen that can be pumped is increased greatly by coating the walls with a frost of gas a few molecular layers thick, such as carbon dioxide, which has a relatively high melting point. Since a monopropellant hydrazine thruster produces large amounts of hydrogen, it is necessary to use this technique. Because only a molecular layer of hydrogen is

cryoabsorbed by the frost layer, a continuous bleeding of carbon dioxide is necessary if hydrogen is being injected periodically into the vacuum chamber. A separate test was conducted to measure the contribution of the carbon dioxide to the mass deposition rate, and it was found that it was about two orders of magnitude less than that for rocket exhaust mass deposition with CO_2 injection. For this reason, no attempt was made to correct the data for this effect. However, it should be remembered that the walls of the chamber are not perfect sinks, and some molecular reflection will occur.

The Molsink chamber has two doors. The upper door is used as a feedthrough for the propulsion system lines and thermal control elements. The door makes a relatively small aperture in the moltrap surface. The bottom door does not have a moltrap surface, and the temperature can rise as high as 200 K because of the external heat conduction. The relatively high temperature of the bottom door caused concern that some material could be scattered back and thus degrade the space simulation. To eliminate this problem, a copper cone was located above the door and cooled with liquid nitrogen or liquid helium as needed. With this technique, one can control the bottom door temperature and maintain the deposited carbon dioxide frost as a very thin film, with any excess being colleced in a "cold bucket" around the rim of the cone (see Fig. 1). More information about the facility can be found in Ref. 1-3.

Propulsion System

A Hamilton-Standard REA 10-18 thruster/valve assembly was made available to JPL by the Air Force Rocket Propulsion Laboratory (AFRPL) for this experiment. At the beginning of the Molsink test, the thruster had only 2353 pulses and 292 sec of on-time as a result of the acceptance test. The cryogenic environment inside the chamber during testing exposes the thruster, valve, and propellant lines to possible freezing. These sensitive items are heated by strip and spot heaters and protected from radiative cooling by appropriate shielding. The heat-conduction losses are small if good insulation and low pressure are maintained in the chamber. The nominal temperatures of the thermally controlled components of the propulsion system are: fuel lines, 20-30°C; filter, 20-30°C; solenoid valve, 20-30°C; catalyst bed, 200°C.

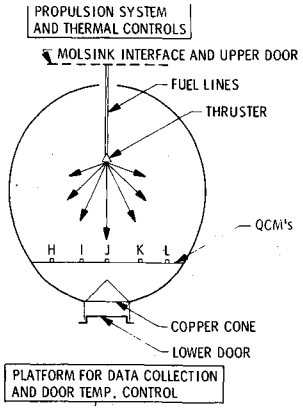

Fig. 1 General arrangement of the different systems at the Molsink (not to scale).

$$\Delta f_1 = C_{M_1}\Delta M_1 + C_{T_1}\Delta T_1$$
$$\Delta f_2 = C_{M_2}\Delta M_2 + C_{T_2}\Delta T_2$$
$$\left.\begin{matrix} C_{M_1} = C_{M_2} \\ C_{T_1} = C_{T_2} \end{matrix}\right\} \text{ if } T_1 = T_2$$
$$\Delta F = \Delta f_1 - \Delta f_2 = C_{M_1}\Delta M_1$$

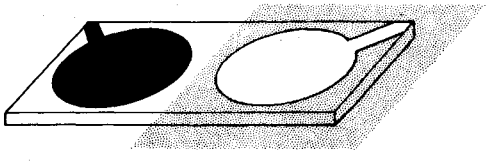

Fig. 2 Doublet QCM.

The propellant feed module was located at the top of the Molsink chamber near the upper door, and the operations were commanded by remote control from the lower floor of the facility, after the propellant tank was pressurized. The feed module also had a piston flowmeter incorporated into the design so that the mass deposition rate could be related to the propellant flow rate.

The propellant feedlines from the module were fed through the upper door and down to the thruster/valve assembly. The engine and the valve were instrumented with seven thermocouples and a coiled coaxial electrical heater. With this arrangement, thermal control of the engine catalyst bed could be maintained, while temperature readings of the throat, catalyst bed, and other locations of interest on the thruster/valve assembly could be obtained. The volume of the pressure tap in the nozzle inlet was eliminated by positioning an appropriate needle in its interior. Also, the CO_2 injection system was fed through the upper door and consisted of a nozzle-plenum assembly located near the top of the chamber. The flow of CO_2 was controlled by a solenoid valve operated by a relay, which, in turn, was energized by a pulse generator synchronized to be out of phase with the engine valve driver system. The CO_2 solenoid valve also could be operated manually, providing a flexible injection system. The CO_2, supplied from a K bottle, was filtered by 20- and 1-μ filters, in order to minimize undesired contamination introduced in the chamber.

QCM Working Principle, Design, and Installation

A QCM consists of an electronic oscillator whose resonance frequency is stabilized by the piezoelectric effect of a quartz crystal. For this series of the tests the AT crystal cut is used, which yields a thickness vibration resonant mode of about 5 MHz. Depending on the angle of the AT cut, the precise resonance frequencies will depend both on the mass deposited on the surface of the crystal and the temperature. If the crystal experiences a variation in temperature ΔT and a mass variation ΔM, the frequency shift can be expressed as

$$\Delta f = C_M \Delta M + C_T \Delta T \tag{1}$$

where C_m and C_T are the mass coefficient and temperature coefficient of the crystal, respectively.

Although the cut angle of the crystal can be chosen so that $C_T = 0$ over some temperature range, it is preferred to employ a temperature-compensated crystal to insure that no undetected temperature effects will occur over the much broader temperature range required for these tests. Bartera[4] conceived such a temperature-compensated crystal which, in spite of its simplicity, provides a very efficient temperature compensation (see Fig. 2).

Consider two crystals, Nos. 1 and 2, both exposed to mass deposition and temperature variation. The corresponding change in frequency can be written as

$$\Delta f_1 = C_{M_1}\Delta M_1 + C_{T_1}\Delta T_1 \tag{2a}$$

$$\Delta f_2 = C_{M_2}\Delta M_2 + C_{T_2}\Delta T_2 \tag{2b}$$

If both crystals have identical piezoelectric properties and are kept at the same temperature, then

$$C_{M_1} = C_{M_2} \quad C_{T_1} = C_{T_2} \quad \Delta T_1 = \Delta T_2 \tag{3}$$

Subtracting Eq. (2) and taking Eq. (3) into account, we have

$$\Delta f = \Delta f_1 - \Delta f_1 = C_{M_1}(\Delta M_1 - \Delta M_2) \tag{4}$$

In addition, if one of the crystals is protected from mass deposits so that $\Delta M_2 = 0$, then we have

$$\Delta f = C_{M_1} \Delta M_1 \tag{5}$$

that is, the beat frequency shift Δf of both crystals can be correlated easily with the mass deposition on one of them.

The condition just described in the preceding paragraph (namely $T_1 = T_2$, identical piezoelectric constants, and $M_2 = 0$) are achieved if one adopts the arrangement described in Fig. 2. A doublet crystal plate is cut and polished. Gold electrodes are deposited on one side, in the form indicated by the figure, whereas a rectangular electrode that is common to both parts of the doublet is used on the other side. Under these premises, and if the crystals are driven at low voltage, one can have two independent crystal oscillators. By protecting one of them from mass deposit with a screen optically thin to the environment radiation, the beat frequency shift of both crystals is given by Eq. (5).

The mass coefficient in Eq. (5) follows quite easily from the relationship of natural frequency of a quartz crystal excited in the thickness shear mode to its thickness. This relationship is given by

$$f = V_{tr}/2t = N/t \tag{6}$$

where V_{tr} is the velocity of the elastic transverse wave in thickness direction, and t is the crystal thickness. For crystals having AT cuts, the constant N is 1.670×10^6 Hz-mm. Differentiating the preceding frequency equation with respect to t, since a change in thickness corresponds to a change in the mass, and using the relation

$$t = m/\rho A = M/\rho \tag{7}$$

where m is the crystal mass, ρ the crystal density, and M the crystal mass per unit area, one obtains

$$dM = -(N\rho/f^2)\,df \tag{8}$$

When the resonant frequency f (Hz) is converted to F_c (MHz) and the density, $\rho = 2.280$ g/cm^3, is introduced into Eq. (8), the following expression results for the mass change per unit area:

$$\Delta M = -[(3.82 \times 10^{-7})/F_c^2]\,\Delta f \tag{9}$$

This is the desired equation, where M is in grams per square centimeter, F_c is in megaHertz, and f is in Hertz. The negative sign in Eq. (9) is arbitrary in that it can be changed in the electronics. Thus, with $F_c = 5.0$, Eq. (9) becomes

$$dM/dt = -1.524 \times 10^{-8}\, df/dt \tag{10}$$

where it is now is expressed as the desired rate equation. With df/dt given in Hertz per second, the mass deposition rate per unit area is in grams per square centimeter-second.

The AT cut for crystals H, I, K, and L was 35°10′, whereas the cut for crystal J was 40°28′. The 40°28′ cut has a small temperature coefficient at low temperatures, i.e., from 10 to 125 K, whereas the 35°10′ cut works best for temperatures of 125 K and above. However, the effectiveness of the temperature compensation design made the crystal cut angle insignificant in the temperature range from 106 to 256 K.

Temperature compensation is achieved by the technique described earlier, and the gold-wire hairbrush mounting absorbs any thermal stresses that otherwise would cause mechanical failure of the crystal; notice that good thermal conductance from the block to the crystal still is maintained. (see Fig. 3). A photograph of a variable-temperature QCM can be seen in Fig. 4. The QCM unit was provided with heaters, which were controlled by a copper-constantan thermocouple located in the proximity of one of the heaters, whereas the crystal temperature was monitored by a similar thermocouple placed at one corner of the crystal. A third thermocouple was located in the crystal mounting block to assess the temperature difference between the crystal and crystal block. The unit was covered with a Teflon block collimator provided with two circular apertures. One of these apertures was used to collect and collimate the oncoming gases, whereas the other was covered with a transparent piece of Mylar.

Five variable-temperature QCM's were mounted on a copper bar located across the chamber, as depicted in Figs. 1

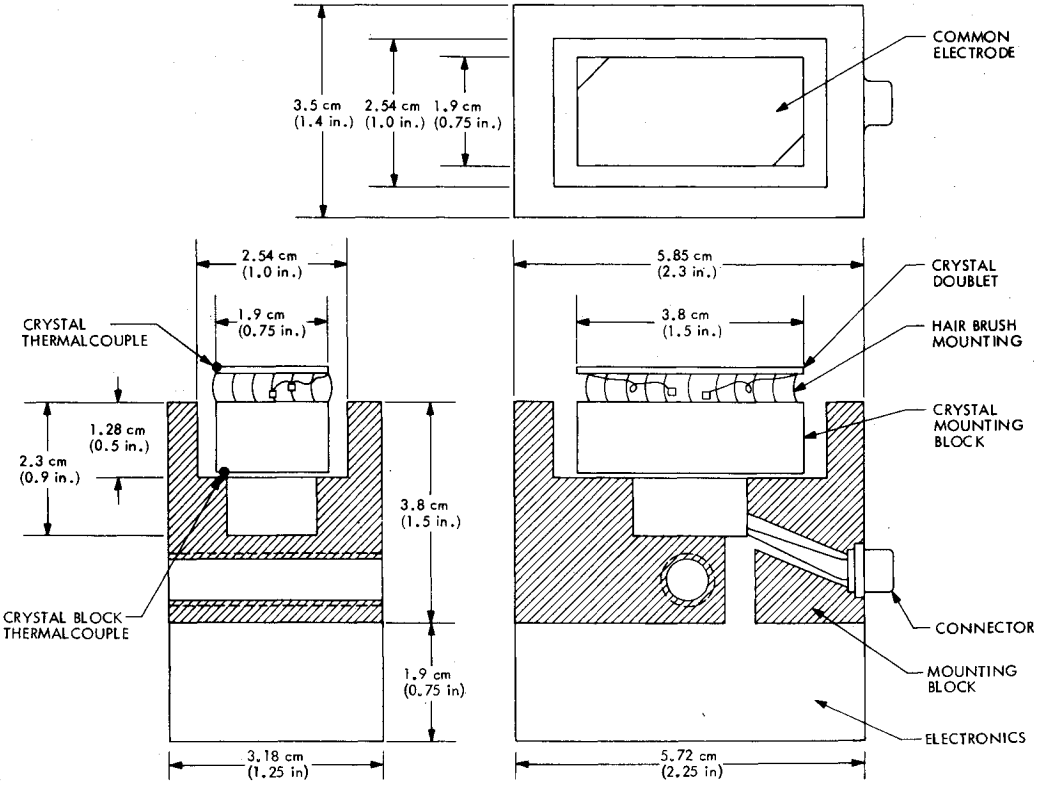

Fig. 3 Schematic diagram of QCM unit.

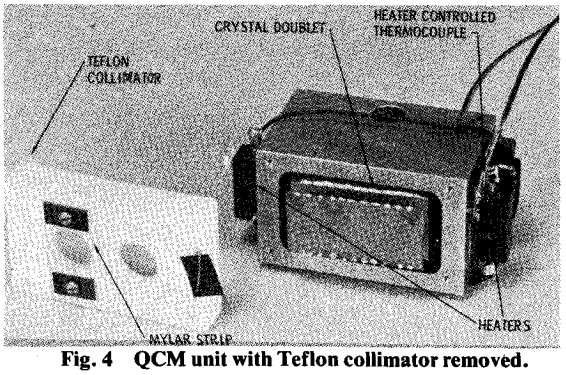

Fig. 4 QCM unit with Teflon collimator removed.

and 5. The QCM's are identified with the letters H, I, J, K, and L and are located nominally at $-30°$, $-15°$, $0°$, $+15°$, $+30°$, respecitvely. The electronics and heater wiring of all of the QCM units were extracted through the bottom door and from there channeled to the data systems and control panels. The copper-constantan thermocouples of all of the QCM's (a total of 16) were fed through a 36-pin connector and then sent to the reference junctions of the data systems and thermal controllers. The heater controlling thermocouples of the variable-temperature QCM's dynamically controlled the temperature of the QCM units. The actual setting of the control point for these heaters was determined by readings from the thermocouples located on the crystals.

Data Systems

The signal from the QCM's was brought out of the chamber, split, and recorded by two separate data systems. The first, or primary, system consisted of the signal being fed into an oscilloscope coupled to a counter, which, in turn, fed into a teletype printer, which produced a permanent record of the crystal frequency, along with other pertinent information. The second, or backup, system consisted of an oscilloscope coupled to a counter, which fed into a digital-to-analog converter and then to strip chart recorders so that a real-time evaluation of the data could be made. The counters for both data systems were set to a frequency accuracy of 0.1 Hz. The accuracy of the data is on the order of $\pm 6.0 \times 10^{-12}$ g/(cm^2-sec). Table 1 shows the number of molecular layers for the gases of interest which would be present due to a frequency change of 1 Hz.

Results

Mass deposition rate data were collected for all variations of thruster parameters at four crystal temperatures: 144, 172, 200, and 228 K. In addition, data were collected for nominal thruster operating conditions at a crystal temperature of 106 K in an effort to condense some NH_3, and at a crystal temperature of 256 K to confirm the expectation that no mass deposition of any species would be seen.[5] It was confirmed that there was no mass deposition at the 256 K crystal temperature. It also was found that the mass deposition rate for a

Table 1 1 Hz = X molecular layers

Gas	X
H_2	4
N_2	0.52
NH_3	1.21
CO_2	0.50
H_2O	1.23
N_2H_4	2.80

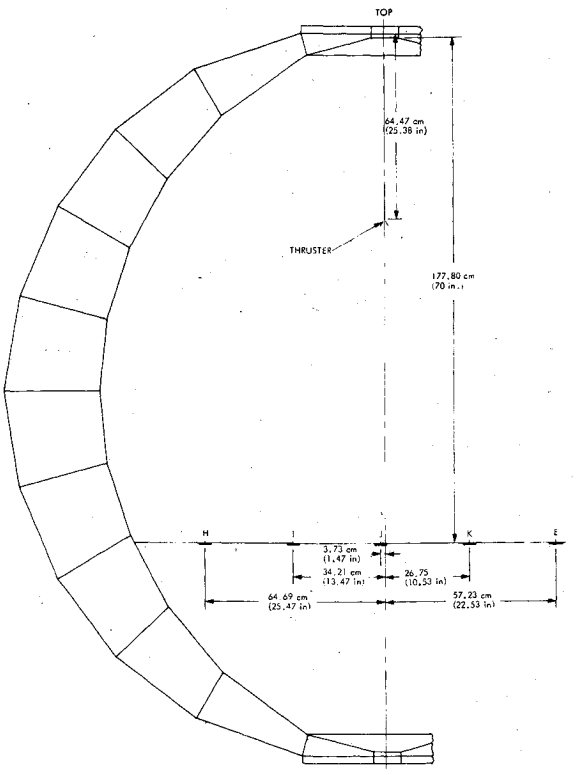

Fig. 5 QCM orientation and thruster position in Molsink chamber.

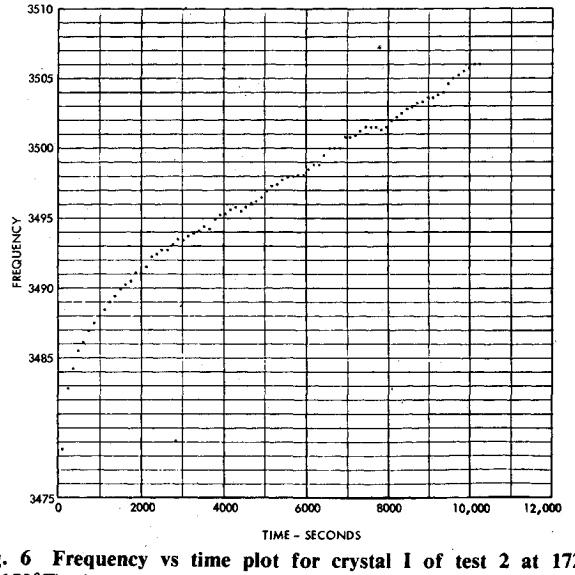

Fig. 6 Frequency vs time plot for crystal I of test 2 at 172 K (−150°F) with nominal duty cycle.

crystal temperature of 228 K was slightly less than the expected accuracy of the combined QCM's and data system. Since the data for crystal temperature of 256 and 228 K do not show any mass deposition, they will not be presented here.

The measured mass deposition rates for the three crystal temperatures 144, 172, and 200 K with various thruster operating conditions are presented in Table 2. The mass deposition rates for the crystals are given in grams per square centimeter-second. The mass deposition rate set off by parentheses indicate the portion of the data where the catalyst bed temperature was traisient, not yet atteining its steady-state value. The transient mass deposition rate was, on the average, 32% higher than that for the steady-state mass deposition rate, which should not be unexpected because of

Table 2 Mass deposition rates at various crystal temperatures and thruster conditions

Test #	Purpose of Test	Crystal Temp. (°K)	Duty Cycle on/off (msec/sec)	No. of Pulses at Start of Test	No. of Pulses During Test	H (gm/cm² sec)	I (gm/cm² sec)	J (gm/cm² sec)	K (gm/cm² sec)	L (gm/cm² sec)
1	Baseline Measuremt.	200	100/10	3353	1000	4.38-12	9.60-12	3.27-11	8.47-12	*
2	" "	172	100/10	4353	1000	*	2.80-11 (6.40-11)	7.87-11 (1.43-10)	1.31-11 (4.00-11)	*
3	" "	144	100/10	5353	334	6.74-10 (1.13-9)	3.49-9 (5.58-9)	4.01-9 (5.84-9)	3.66-9 (5.61-9)	*
4	" "	106	100/10	26558	302	1.98-8 (2.67-8)	7.13-8 (8.18-8)	7.54-8	8.25-9 (1.28-8)	6.10-9 (9.61-9)
5	Effect of Short Pulse	200	25/5	9515	2062	*	*	*	*	*
6	" " "	172	25/5	6693	2222	1.69-12	1.44-11	3.26-11 (5.30-11)	1.00-11	*
7	" " "	144	25/5	14034	2059	2.69-10 (3.27-10)	1.94-9 (2.51-9)	2.07-9 (2.62-9)	1.67-9 (2.62-9)	1.09-10
8	Effect of Long Pulse	200	200/20	18882	408	*	*	*	*	*
9	" " " "	172	200/20	18298	410	*	2.49-11 (3.72-11)	1.13-10 (1.30-10)	3.23-11 (3.81-11)	*
10	" " " "	144	200/20	19788	419	3.22-10 (3.71-10)	1.87-9 (2.30-9)	2.58-9 (2.91-9)	2.15-9 (2.35-9)	1.23-10 (1.30-10)
11	Effect of Catalytic Bed Temp at Start 70°F	172	100/10	22029	580	(1.79-12)	(3.08-11)	(1.04-10)	(1.31-11)	*
12	" " " 200°F	172	100/10	20398	590	(1.79-11)	3.24-11)	(1.17-10)	(2.46-11)	*
13	" " " 400°F	172	100/10	26288	270	(1.30-12)	(3.80-11)	(1.22-10)	(2.22-11)	(2.02-11)
14	" " " 600°F	172	100/10	23449	270	*	*	(1.05-10)	(1.25-11)	*
15	Baseline Remeasure	200	100/10	25159	769	*	5.24-11	*	*	*
16	" "	144	100/10	23989	750	6.02-10 (7.82-10)	2.60-9 (3.04-9)	2.89-9 (3.51-9)	2.37-9 (2.59-9)	1.76-10 (2.18-10)
17	Mil Spec Prop. + 1.1% H_2O	200	100/10	26860	774	2.53-12	*	9.82-12 (1.69-11)	*	*
18	" " "	172	100/10	29136	767	2.06-11	3.60-11	1.14-10	2.75-11	*
19	" " "	144	100/10	27994	782	7.01-10 (7.19-10)	3.92-9 (4.08-9)	4.39-9 (4.80-9)	3.92-9 (3.96-9)	2.33-10 (3.44-10)
20	Effect of Ageing	200	100/10	132430	990	8.27-12 (1.23-11)	5.34-11 (5.54-11)	6.02-11 (6.72-11)	5.26-11 (5.54-11)	*
21	" " "	172	100/10	131220	940	1.49-11 (2.41-11)	8.32-11 (1.10-10)	1.11-10	8.05-11 (1.06-10)	1.46-11
22	" " "	144	100/10	134210	1024	2.21-10 (4.50-10)	1.16-9 (1.73-9)	1.50-9 (1.99-9)	1.05-9 (1.30-9)	4.98-11

*Data were of less quality and therefore were omitted.

unburned N_2H_4 and NH_3 present during startup. The first four tests were the baseline measurements at the nominal duty cycle of 100 msec on and 10 sec off at four crystal temperatures. In tests 5-7, the duty cycle was changed to 25 msec on and 5 sec off to assess the effect of a short pulse width. Similarly, tests 8-10 had a duty cycle of 200 msec on and 20 sec off to measure the effect of a long pulse width. Tests 11-14 were made a one crystal temperature, 172 K. The purpose of these tests was to see how the starting temperature of the catalyst bed affects the mass deposition rate during the transient temperature portion of the startup. Tests 15 and 16 were rebaseline measurements at 144 and 200 K crystal temperature for the nominal duty cycle. The propellant for tests 17-19 had 1.1% water by weight added to the 0.7% already present in an effort to see what effect water had on mass deposition rates at these temperatures. The last group of tests (20-22) was a rebaseline measurement after the thruster had been aged approximately 10^5 pulses after the completion of the previous test. To illustrate the data quality, Fig. 6, which is a frequency vs time plot for crystal I at a temperature of 172 K (see test 2 of Table 2), has been included. It should be noted that the associated mass deposition rate for this plot, 2.80×10^{-11} g/(cm²-sec) ,is typical of the data quality for all of the data shown. The plots for mass deposition rates equal to or greater than 1.00×10^{-10} g/(cm²-sec) showed no visible data scatter, The data accuracy was on the order of 6.0×10^{-12} g/cm²-sec), as stated before. It should be pointed out that for tests 1-4 the catalyst bed temperature was about 450 C. Before test 5 was started, the catalyst bed heater failed and had to be replaced by a coiled resistance heater, which

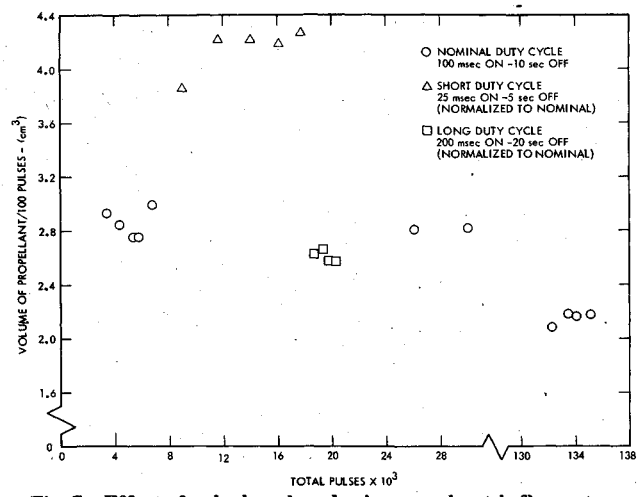

Fig. 7 Effect of pulse length and aging on volumtric flow rate.

required the removal of the thruster heat shield. This caused additional radiative heat transfer, which resulted in a catalyst bed temperature reduction at steady state to about 360°C for all of the remaining tests.

As described earlier, a piston flowmeter was incorporated into the propulsion feed module. The inlet pressure was maintained and constantly monitored at a value of 78.6 N/cm^2, which gives a chamber pressure of 57.9 N/cm^2 and a thrust of 0.44 N for the thruster when it was new. Figure 7 shows the volumetric flow rate (cm^3/100 pulses) of the thruster vs the total number of pulses. The change of volumetric flow rate as a function of pulse length and aging is quite evident. The high flow rate for the short pulse is probably because there is insufficient time for the chamber pressure to build up, which would retard the flow rate. The slightly lower flow rate for the long pulse is caused by the opposite effect. The flow rate for the nominal duty cycle seems to be constant for at least the first 3×10^4 pulses. After 1.3×10^5 pulses, the volumetric flow rate is down about 25%. It is speculated that the catalyst bed is packing tighter against the regaining screen, thus producing a greater pressure drop across the bed, with a corresponding drop in flow rate.

The effect of pulse length on mass deposition is shown in Fig. 8. It is quite apparent that the pulse length has little effect on the contamination rate. The effect is smaller yet if the reduction of mass deposition rate with age is taken into account (see Fig. 10).

The mass deposition rate, as a function of crystal temperature, varies about four orders of magnitude for a variation of temperature from 106 to 200 K. These results are presented in Fig. 9. The significant point to be noted here is the marked increased in mass deposition rate for crystal temperatures below 172 K. For the crystal temperatures of 200 and 172 K, the most likely contaminants are aniline and unburned hydrazine. The small increase in mass deposition rate from 200 to 172 K indicates there are probably no new contaminants at 172 K, as compared to those present at 200 K. The marked increase in mass deposition rate for 144 K is probably due to water capture. Water will stick for crystal temperatures below about 162 K at these pressures (see Table 3). Similarly, the increase in mass deposition rate at 106 K is caused by the fact that ammonia now is captured by the crystal. Ammonia capture at a chamber pressure of about 10^{-4} N/M^2 will occur approximately at 106 K. (A complete listing of approximate condensation temperatures for the plume exhaust products is given in Table 3).

The mass deposition rate is shown for the nominal duty cycle at a crystal temperature of 144 K as a function of thruster age in Fig. 10. The decrease in mass deposition on the crystals with age can be explained only by the break-in of the thruster wherein the percentage decomposition of NH_3 increases, producing a larger percentage of H_2 and N_2, which will not condense on the crystals at this temperature. This is consistent with the decrease of flow rate with time due to the

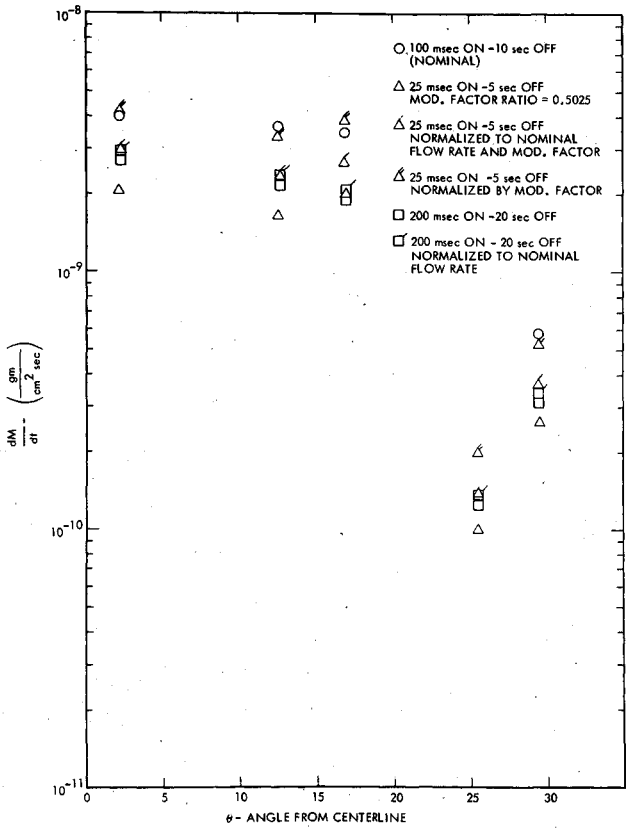

Fig. 8 Effect of duty cycle on mass deposition rate at a crystal temperature of 144 K.

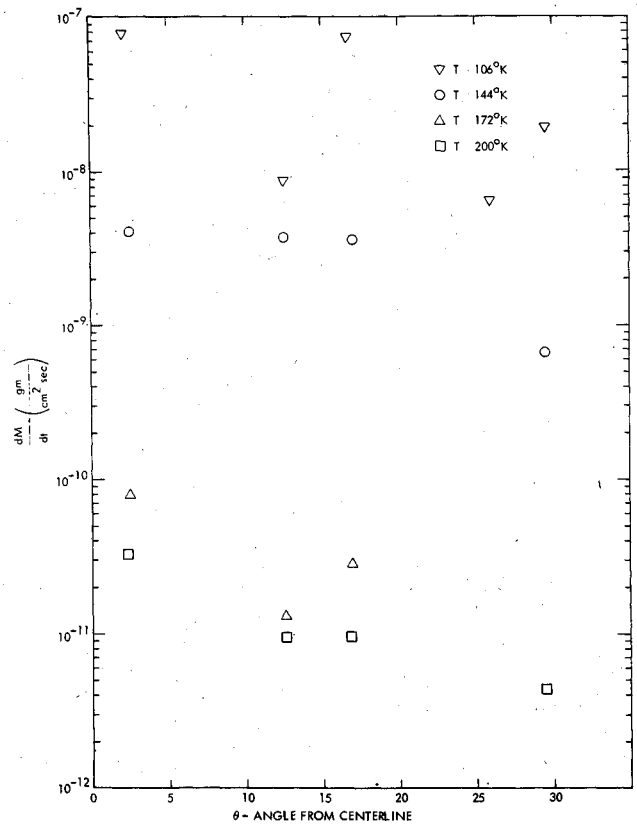

Fig. 9 Effect of crystal temperature on mass deposition rate.

Table 3 Capture temperature for exhaust plume products at approximately 10^{-4} N/m^2

Gas	Temperature, K
Ammonia NH_3	102
Aniline CH_x	?
Carbon dioxide CO_2	86
Hydrazine N_2H_4	?
Hydrogen H_2	4
Nitrogen N_2	27
Water H_2O	162

cataylst bed becoming packed more tightly against the regaining screen, thus producing greater NH_3 decomposition. A significant observation , especially after the 10^5 pulses of aging, was that the number of pulses which could be run before the chamber avalanched continually decreased with time. This supports the contention that the percentage decomposition of NH_3 increased with time. The "avalanche effect" can be explained quite simply. If for some reason the hydrogen sorption onto the wall is diminished, additional hydrogen injected into the chamber will reduce the vacuum, resulting in an increase in heat-conduction losses. This, in turn, causes an additional warming of the walls which results in hydrogen desorption. This phenomenon has an exponential growth and results in the rapid desorption of hydrogen from the walls occurring within a matter of seconds and is referred to as the "avalanche effect." This happened only a few times during testing since it was induced externally between tests when the chamber seemed to be "loading up" with hydrogen. The avalanche effect created an upper limit for the Molsink chamber pressure of 4.0×10^{-3} N/m^2, whereas the starting pressure was on the order of 1.33×10^{-4} N/m^2.

The Mil Spec propellant assayed at 0.7% water. A test to measure the effect of the water in the propellant was performed by adding 1.1% water (nominally 1%) to the propellant and then comparing the results to the tests for Mil Spec propellant with only 0.7% water. The results are shown in Fig. 11. The Mil Spec plus 1.1% water showed a very uniform increase of mass deposition rate with angle over that for the Mil Spec of a factor of 15.

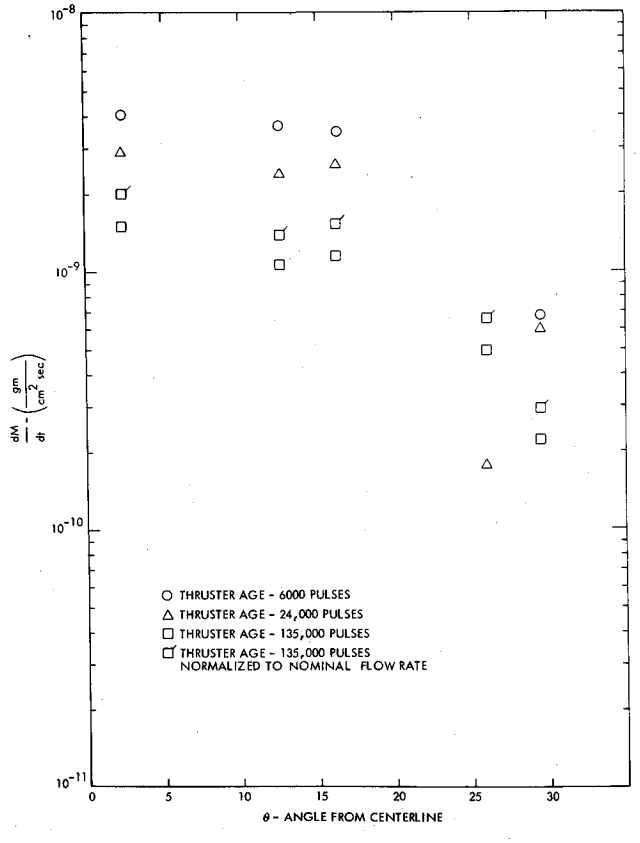

Fig. 10 Effect of thruster aging on mass deposition rate at a crystal temperature of 144 K.

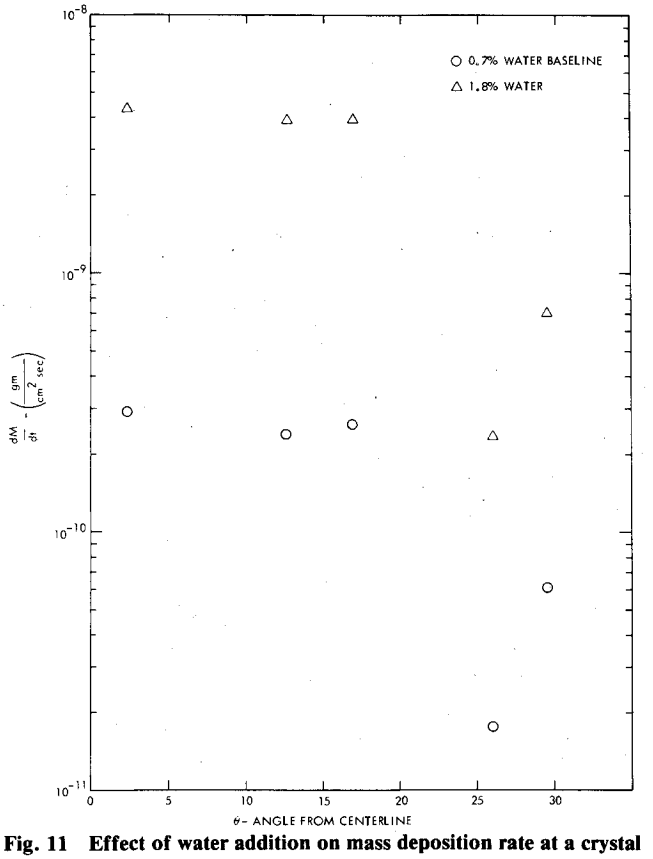

Fig. 11 Effect of water addition on mass deposition rate at a crystal temperature of 144 K.

Conclusions and Future Work

The data presented here indicate that the pulse length and aging have very little effect on contamination, although it generally is recognized that longer pulse lengths and thruster age reduce the contamination level. The purity of the propellant, at least from the standpoint of water content, can be seen to have a large effect on contamination. Finally, as clearly shown by the data, the best way of reducing contamination of sensitive spacecraft surfaces is to maintain a temperature of 170 K or higher.

In order to determine the types and amounts of contaminants present on the crystals, two kinds of additional measurements should be made. First, desorption rate measurements at a number of isotherms will give data for the mixture condensed on the crystals. (Actually, this was done already in conjunction with this test, and individual species could be seen although they could not as yet be identified.) Secondly, a capture coefficient experiment (which presently is being done) in which the mass deposition rate of a molecular beam of pure gases and of gas mixtures, consistent with the exhaust from a hydrazine monopropellant thruster, is calibrated at a low crystal temperature. Then the crystal temperature is increased at a given temperature intervals, and the fraction of flow deposited is meausred. This fraction is defined as the capture coefficient. Also, desorption rate measurements will be made, and an attempt at predicting what was on the crystals in the monopropellant tests will be made by combining these two results.

Acknowledgment

This paper presents the results of one phase of research carried out at the Jet Propulsion Laboratory, California

Institute of Technology, for the U.S. Air Force Rocket Propulsion Laboratory (Project Order No. 5730-75-6), under Contract NAS 7-100, sponsored by NASA.

References

[1] Stephens, J.B., "Spacecraft Mechanism Testing in the Molsink Facility," *Proceedings of the 4th Aerospace Mechanisms Symposium*, edited by G.G. Herzl and M.J. Buehler, Jet Propulsion Lab., Pasadena, Calif., TM 33-425, Jan. 15, 1970.

[2] Stephens, J.B., "Molecular Sink," *Research/Development*, Vol. 18, July 1967, pp. 42-44.

[3] Stephens, J.B., "Space Molecular Sink Simulator Facility Design," *Journal of Spacecraft and Rockets*, Vol. 3, June 1966, pp. 844-848.

[4] Bartera, R.E., "Quartz Crystal Oscillator Apparatus for Measuring Mass Accreation and Temperature Independently of Each Other," Patent Case 11279, Jet Propulsion Lab., Pasadena, Calif., April 29, 1975.

[5] Chirivella, J.E., "Hydrazine Engine Plume Contamination Mapping," Air Force Rocket Propulsion Lab., AFRPL TR-75-16, Oct. 1975.